

# Supplementary file – X-photon 3D lithography by fs-oscillators: wavelength-independent and photoinitiator-free

Dimitra Ladika<sup>1 2 \* †</sup>, Antanas Butkus<sup>3 \*</sup>, Vasileia Melissinaki<sup>1</sup>, Edvinas Skliutas<sup>3</sup>,  
Elmina Kabouraki<sup>1</sup>, Saulius Juodkazis<sup>3 4 5 †</sup>, Maria Farsari<sup>1 †</sup>, and Mangirdas Malinauskas<sup>3 †</sup>

<sup>1</sup>*Institute of Electronic Structure and Laser, Foundation for Research and Technology-Hellas, 70013 Heraklion, Greece*

<sup>2</sup>*Department of Materials Science and Technology, University of Crete, 70013, Heraklion, Crete*

<sup>3</sup>*Laser Research Center, Faculty of Physics, Vilnius University, Saulėtekio Ave. 10, LT-10223 Vilnius, Lithuania*

<sup>4</sup>*Optical Sciences Centre and ARC Training Centre in Surface Engineering for Advanced Materials (SEAM), School of Science, Swinburne University of Technology, Melbourne, Australia*

<sup>5</sup>*WRH Program International Research Frontiers Initiative (IRFI) Tokyo Institute of Technology, Nagatsuta-cho, Midori-ku, Yokohama, Japan*

\*These authors contributed equally to this work.

†Correspondence to: Saulius Juodkazis: [sjuodkazis@swin.edu.au](mailto:sjuodkazis@swin.edu.au), Maria Farsari: [mfarsari@iesl.forth.gr](mailto:mfarsari@iesl.forth.gr), Mangirdas Malinauskas: [mangirdas.malinauskas@ff.vu.lt](mailto:mangirdas.malinauskas@ff.vu.lt)

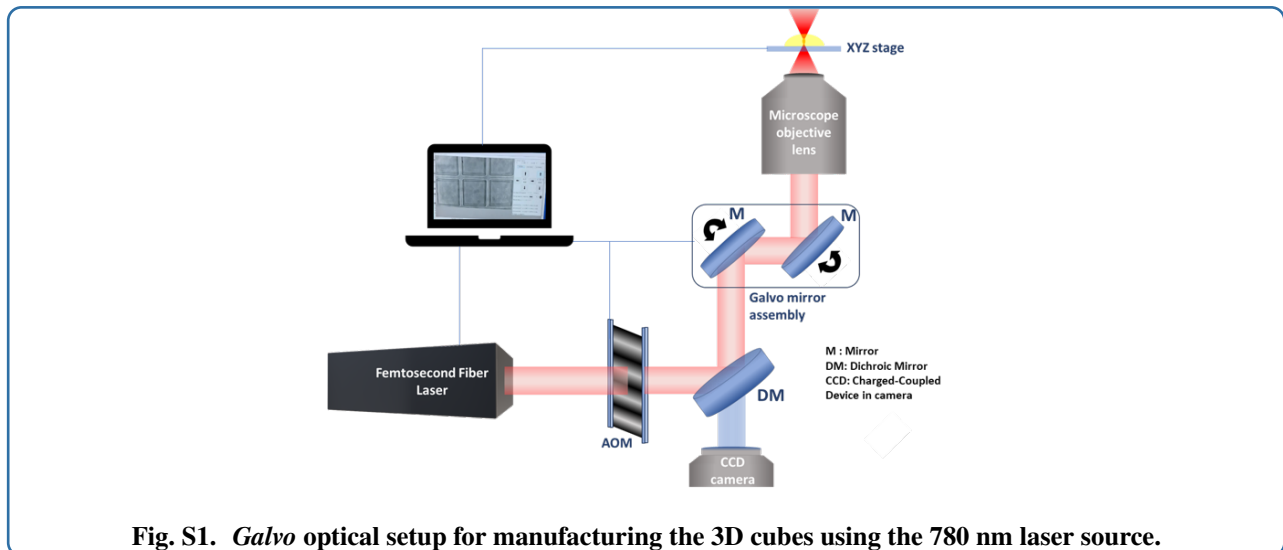
Specific details or additional information can be acquired contacting corresponding authors upon request.



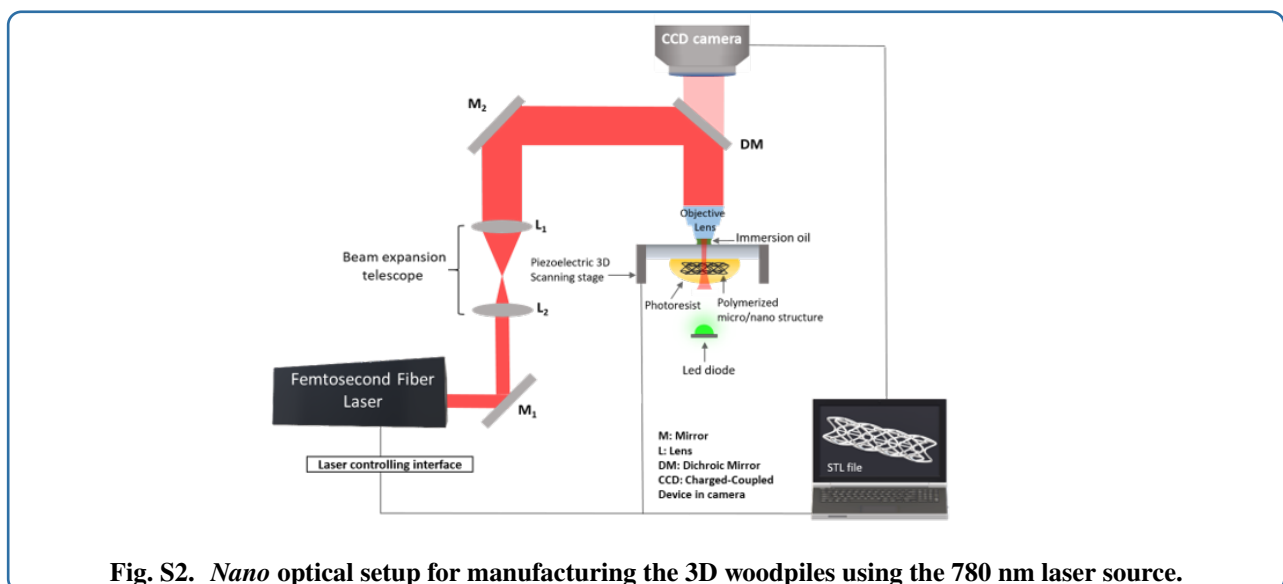
## Experimental setups using the 780 nm laser source

Two experimental optical setups were used to fabricate 3D micro-/nanostructures utilising the 780 nm laser source. For both setups the same laser source was utilised and is mentioned in the main text. The beam is split in two parts by a beam splitter (70/30) and then two sub-setups are developed. For ease of reference, the two sub-setups are presented as two different ones, below. Specifically, in Fig. S1 the *Galvo* apparatus is presented and was used for the fabrication of the 3D cubes. An acousto-optic modulator is used as a shutter, during the fabrication process.

In Fig. S2 the *Nano* apparatus is presented and was used for the fabrication of the 3D woodpiles. Additional to the

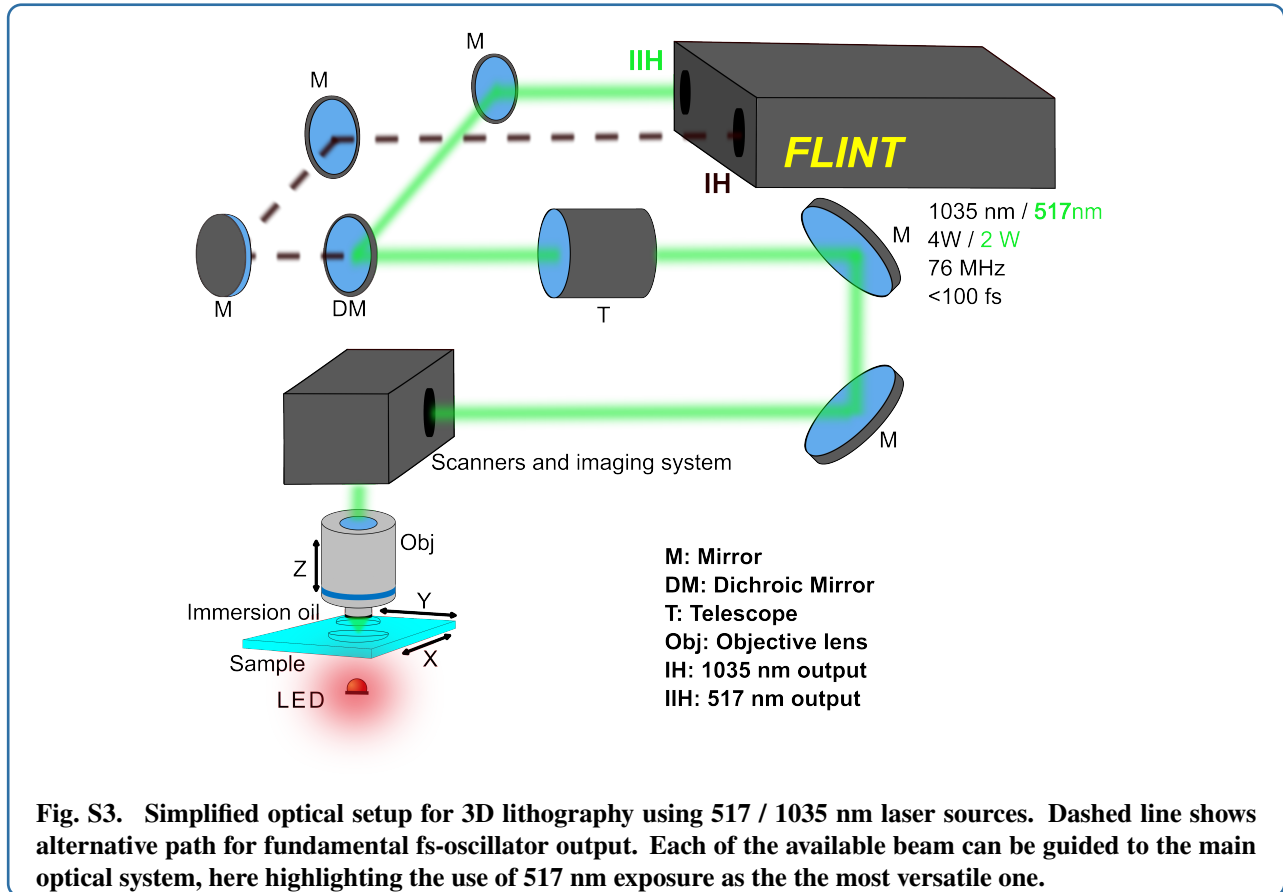


information mentioned in the main text, a telescope is included in the setup, in order to adjust the beam size to the pupil entrance of the objective lens in use. Also, a mechanical shutter is added in the optical path, for controlling the beam during the fabrication. A CCD camera for the imaging of the fabrication process is also adapted in both setups.



### Experimental setup using 517 nm and 1035 nm laser source

Structuring with oscillator having exposure centered at 517 nm and 1035 nm wavelengths was realized with commercial Laser Nanofactory (Femtika Ltd.) setup. Simplified optical scheme is depicted in Fig. S3, where either fundamental (1035 nm) or second harmonic (517 nm) Yb-based fs-oscillator (Flint, Light Conversion Ltd.) output is being delivered to the objective lens through dichroic mirror.



## Exposure parameters in the performed study

Experimental details for all exploited wavelengths are presented in Table S1. Losses of employed objective lenses used for MPL are taken from the manufacturer based on typical transmission curves. Even though previous in-house estimations for specific objectives showed slightly smaller values for some spectral regions [1], yet immersion oil was not used in the measurements which arguably may not accurately reflect existing performance of the objective lens during MPL fabrication. Specifically, datasheet transmission of 63x/1.4 NA oil obj (Plan- Apochromat, Zeiss) at exposures 517 nm and 1035 nm results in respectively, 0.88 and 0.35 [2], while used 100x/1.4 NA oil obj (Plan- Apochromat, Zeiss) at 780 nm wavelength is of 0.75 [3]. Accordingly, dry Mitutoyo M Plan Apo HR 50x/0.75 NA objective lens transmission at 1035 nm wavelength is estimated to be 0.45 [4].

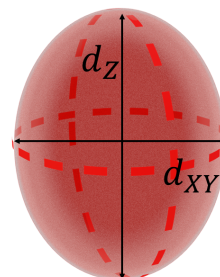
Table S1: Employed experimental conditions for each oscillator wavelength  $\lambda$  : objective lens (Obj), transmission of the objective ( $T$ ), repetition rate ( $R$ ), scanning velocity ( $v$ ), power delivered to the obj ( $P$ ) and estimated exposure Intensity ( $I$ ) which was varied across the focus.  $\tau$  denotes pulse duration,  $r_\lambda$  - wavelength specific focal spot size radius (see table S2).

$\lambda$ (nm)	Structure	Obj	$T$	$R$ (MHz)	$v$ ( $\mu\text{m/s}$ )	$P$ (mW)	$I = \frac{2PT}{R\tau\pi r_\lambda^2}$ ( $\text{TW/cm}^2$ )
780	Cubes	40x/0.95 NA	0.8	80	5	75-200	0.58-1.55
		100x/1.4 NA	0.75		30	20.5-25	0.96-1.18
517	3D Woodpiles	63x/1.4 NA	0.88	76	30-10 <sup>5</sup>	1.5-67	0.22-9.73
1035			0.35		15	205	2.95
		50x/0.75 NA	0.45		5	700	3.72

Next, the evaluation of exposed dimensions (volumes) based on elliptical Gaussian intensity profile under high 1.4 NA focusing at different incident laser wavelengths are presented in Table S2. We take  $n_0 = 1.5$  for SZ2080<sup>TM</sup> [5] in assessing longitudinal ellipsoid length. Parameter calculations present here are based on previously reported nomenclature [6]. Alternatively, exposure dimensions could be evaluated using other existing models, e.g taking Abbe's criterion which argues lateral exposure profile to be defined at full width at half maximum (FWHM) [7] resulting in spot size of  $d_{XY} = \frac{\lambda}{2NA}$  corresponding to  $d_{XY} = 362$  nm ( $\lambda = 517$  nm),  $d_{XY} = 546$  nm ( $\lambda = 780$  nm),  $d_{XY} = 725$  nm ( $\lambda = 1035$  nm). Note, we use Rayleigh criterion  $d_{XY} = \frac{1.22\lambda}{NA}$ , which assumes intensity profile length from maximum to minimum in lateral exposure direction. Therefore, calculations requiring focal spot area estimation (e.g intensity, fluence) are subject to have different absolute values depending on the chosen definition for the exposed volume dimensions, yet processing trends observed herein remain the same. Additional note should be taken, that the exposed volume is a spatial intensity distribution (photon density) but not adequate to the photo-modified region or the final produced voxel which is the result affected by of all the before mentioned processes.

Table S2: Estimated exposure volume dimensions in SZ2080<sup>TM</sup> for all different wavelengths at 1.4 NA focusing conditions.

	$d_{XY}$ (nm)	$d_Z$ (nm)	$V$ ( $\mu\text{m}^3$ )
Formula	$\frac{1.22\lambda}{NA}$	$\frac{1.22n_0\lambda}{NA^2}$	$\frac{\pi d_{XY}^2 d_Z}{6}$
$\lambda$ (nm)			
517	451	483	0.10
780	680	728	0.34
1035	902	966	0.79

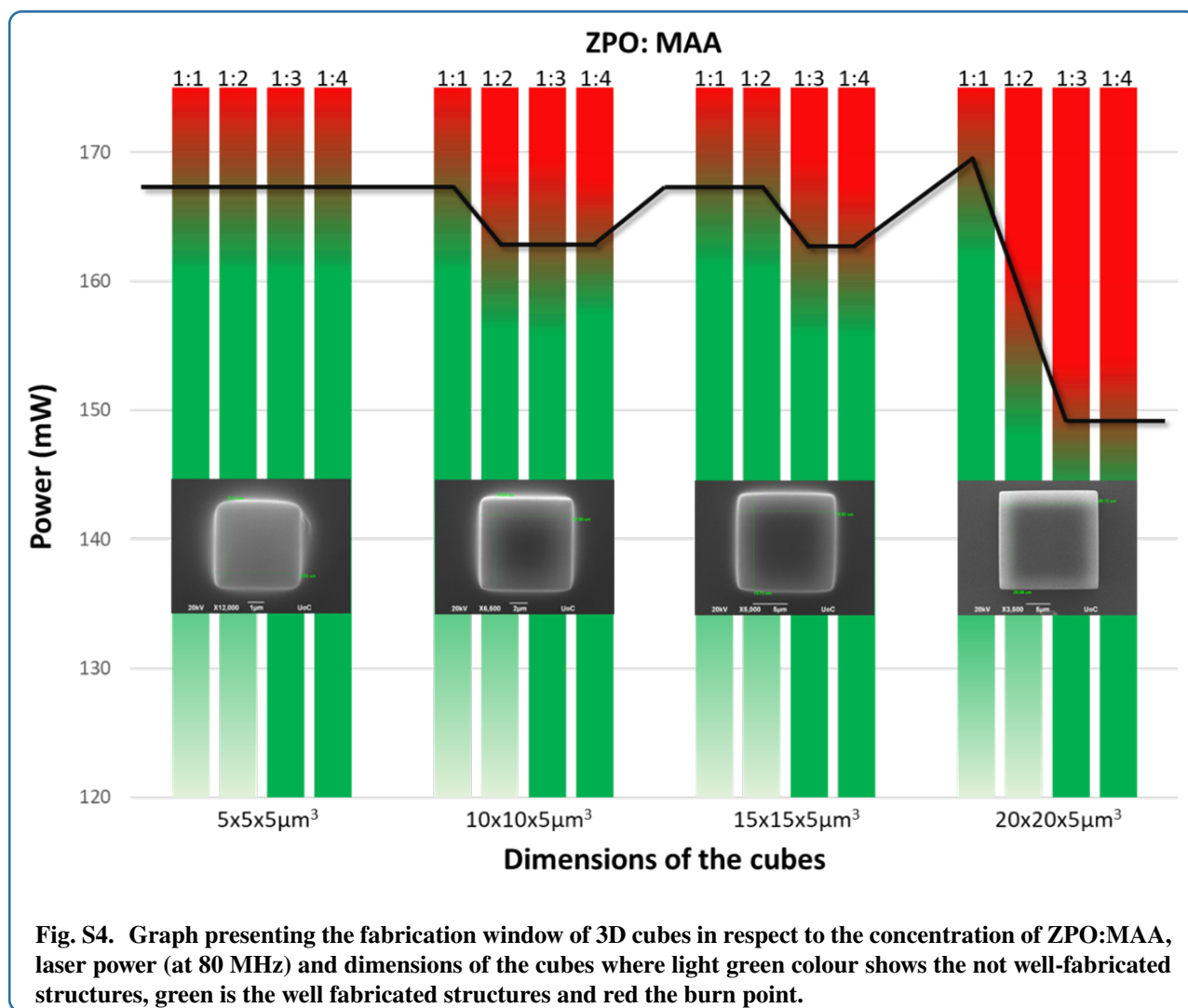


## Non-photosensitized structuring of compositions with various inorganic-organic ratios

Non-photosensitized SZ2080<sup>TM</sup> was successfully photo-polymerized with 780 nm laser beam. The *galvo* apparatus was used to fabricate cubes with different dimensions, namely  $5 \times 5 \times 5 \mu\text{m}^3$ ,  $10 \times 10 \times 5 \mu\text{m}^3$ ,  $15 \times 15 \times 5 \mu\text{m}^3$  and  $20 \times 20 \times 5 \mu\text{m}^3$ . Different molar concentrations of ZPO: MAA (1:1,1:2,1:3,1:4) were used in order to investigate how the dimension (volume) of the structure vs the concentration of MAA in the material affects the process DFW of the material (Fig. S4). The cubes were fabricated with laser powers ranging from 120 mW to 175 mW and with scanning velocity of  $5 \mu\text{m/s}$ . The results show that larger structures ( $20 \times 20 \mu\text{m}^2$ ) are fabricated more accurately than the smaller ones ( $5 \times 5 \mu\text{m}^2$ ). On the other hand, existing local heat accumulation due to tens-of-MHz repetition rate (introduced in the main text Discussion section) is more evident for structures requiring larger scanning volume, hence leading to faster energy deposition reaching dielectric breakdown conditions. A more detailed research would be needed for explaining specifics of why structures more reliably retain design geometry at larger dimensions. The insight is that the energy introduced in larger volume has lesser area-to-volume ratio for the heat to dissipate, thus resulting in denser polymerized object and at the same time reaching the breakdown conditions faster.

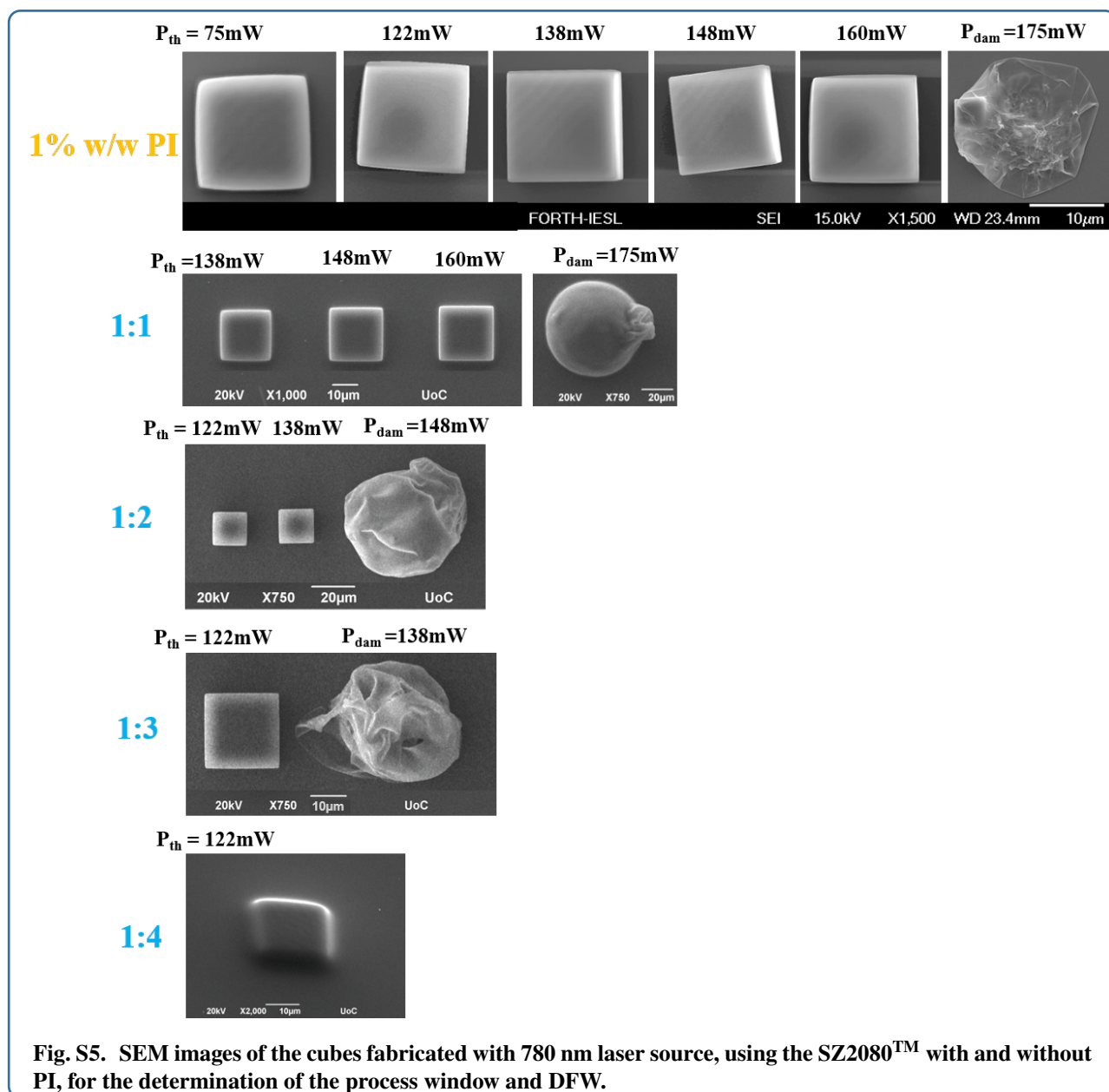
In order to obtain the DFW for the 780 nm laser source in respect to the varied materials concentrations, 3D cubes were fabricated and presented in Fig. S5. These cubes were used for the DFW to be evaluated, shown in Figure 2(B). in the main text. Specifically, below the polymerization threshold for each material, no survived structure was observed while for power values over the damage thresholds, only burning (explosions) of the material was observed resulting into uncontrolled polymerization.

The increased molar concentration of the inorganic component would potentially achieve higher refractive index and mechanical strength of the fabricated 3D structures. However, the higher molar concentration of the inorganic component would result in a material that is more difficult to process compared to the one with higher concentration of the organic part due to more available cross-linking bonds. Additionally, a material with high molar concentration of the organic part would be suitable for the fabrication of high resolved features but at the same time with increased probability of shrinking. Finally, materials for 3D nanolithography that comprise of high concentration of inorganic components are usually biocompatible and resilient to high temperatures, making them suitable for bio-applications and calcination, respectively.



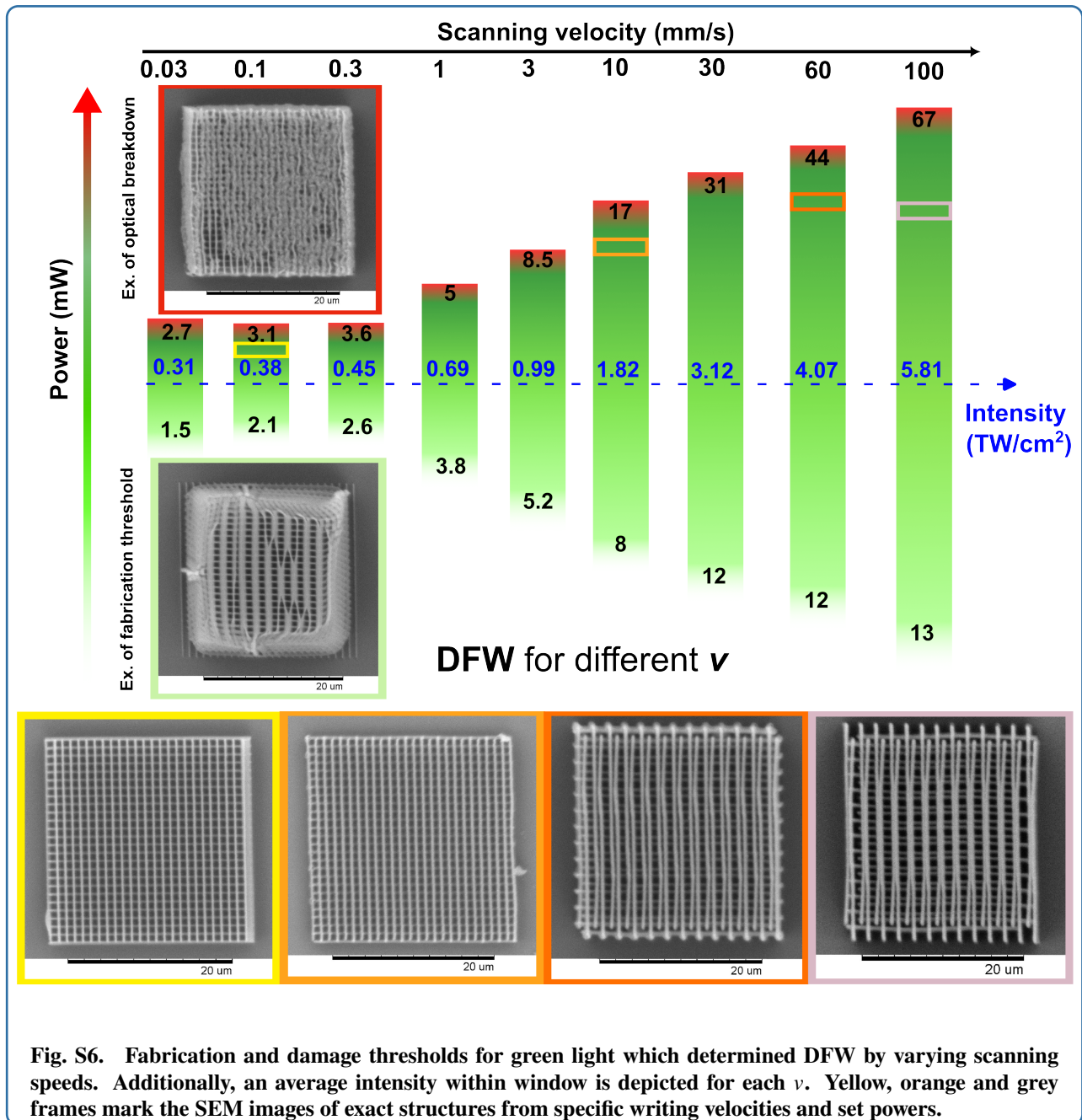
### Dynamic fabrication window for 517 nm wavelength at different writing velocities

DFW for green (517 nm) light was determined at various scanning speeds ranging from 30 to  $10^5$   $\mu\text{m}/\text{s}$ . It showed the highest potential in fast writing speeds - depicted in Fig. S6. An average intensity as the middle value in between DFW indicates its growth in respect in scanning speed (inversely proportional to the exposure time). As it is seen while the exposure time is varied by 4 order of magnitudes (from 30 to  $10^5$   $\mu\text{m}/\text{s}$ ) the intensity is increased by roughly just one order (from 0.31 to 5.81  $\text{TW}/\text{cm}^2$ ). This gives a hint that the polymerization at higher speeds is enabling more efficient energy delivery as the heat dissipation is enhanced by expanded exposed volume corresponding to surface area for diffusion. Thus, the higher scanning speeds resulting in shorter exposure duration empowers mitigation of heat accumulation related effects. At the same time the higher intensity ensures more efficient non-linear absorption which probability phenomenon by nature dependant on photon flux density. Extrapolating from the obtained results, with the increase of scanning speed by 10 times the intensity needs to be adjusted by increasing it 2 – 3 times. Thus, within the studied range total increase in translation speed of 3 333 times required increase of intensity by 19 times. It is noted, that the increase of scanning



speed linearly directly decreases the fabrication time, while the diminished growth of required intensity reduces the power requirement for employed non-amplified laser sources. Such trend correlates with the expansion of the DFW at faster translations as well. The findings are useful as a guide for power-to-speed scaling laws and promising for the rapid optical 3D nano-lithography using high-repetition rate femtosecond pulses.

It should be noted that the light intensities for polymerization and fabrication thresholds are related, yet not exactly adequate parameters. The polymerization threshold stands for irreversible modification of the material, while the fabrication threshold means the survivable structures, which is both geometry and filling ratio (porosity) dependent. For e.g. the fine suspended lines will have higher fabrication threshold in respect to a densely overlapping woodpile structure where each of the line is connected to perpendicular ones serving as support structures. Thus, though each



of them are useful for deterministic studies, yet the first one is more for studying the photo-chemical mechanisms of light-matter interaction and the later one defines the optimization for the additive manufacturing of specific architectures.

### MPL utilizing 1035 nm oscillator exposure at moderate (NA = 0.75) focusing conditions

Achieving polymerization with non-photosensitive SZ2080™ is not limited to high NA optics which are typically used with immersion oils. Here, we show a proof of concept at Fig. S7, where sample fabrication is performed with Mitutoyo M Plan Apo HR 50x/0.75 NA objective lens. Yet significant limitations are noted, specifically only at low scanning velocities a controllable fabrication is achieved without inducing optical breakdown conditions. As a result of larger focus spot size compared with 1.4 NA objective lens, required power for inducing localized cross-linking reaches 700 mW, where intensity  $I$  accounting for objective losses [4] then becomes  $3.72 \text{ TW/cm}^2$ , which is consistent with values at 1.4 NA conditions exploiting the same 1035 nm wavelength ( $\sim 3 \text{ TW/cm}^2$ ).

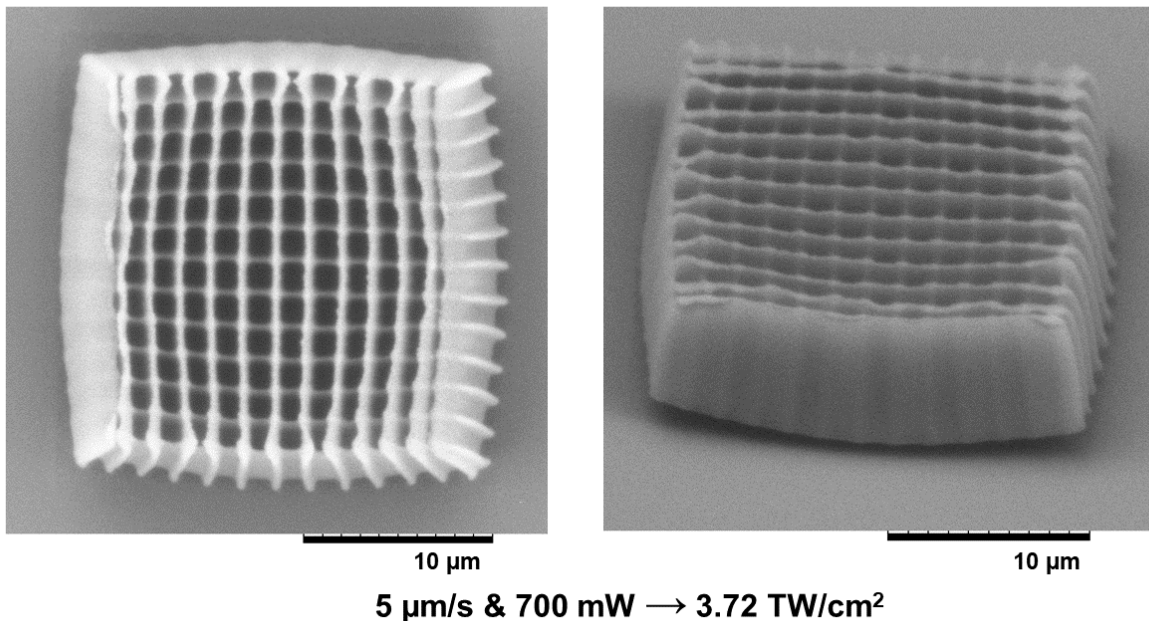


**Fig. S7.** SEM images of structure fabricated with 1035 nm oscillator exposure and dry objective (NA = 0.75) focusing. Note the average power is significantly higher (700 mW instead of 200 mW), yet the corresponding intensity is consistent with immersion oil objective focusing (NA = 1.4) as the exposed volume changes accordingly.

---

## References

- [1] Samsonas, D. et al. 3D nanopolymerization and damage threshold dependence on laser wavelength and pulse duration. *Nanophotonics* **12**, 1537–1548 (2023).
- [2] Transmittance curve. <https://www.micro-shop.zeiss.com/en/us/shop/objectives/420782-9900-000/Objective-Plan-Apochromat-63x-1.4-Oil-DIC-M27>. Accessed on 2024-07-05.
- [3] Transmittance curve. <https://www.micro-shop.zeiss.com/en/us/shop/objectives/420790-9901-000/Objective-Plan-Apochromat-100x-1.40-Oil-M27>. Accessed on 2024-07-05.
- [4] Typical Transmission for M Plan Apo. <https://www.edmundoptics.com.sg/f/mitutoyo-infinity-corrected-long-working-distance-objectives/12298/>. Accessed on 2024-07-05.
- [5] Ovsianikov, A. et al. Ultra-low shrinkage hybrid photosensitive material for two-photon polymerization microfabrication. *ACS Nano* **2**, 2257–2262 (2008).
- [6] Skliutas, E. et al. Polymerization mechanisms initiated by spatio-temporally confined light. *Nanophotonics* **10**, 1211–1242 (2021).
- [7] Fischer, J. & Wegener, M. Three-dimensional optical laser lithography beyond the diffraction limit. *Laser & Photonics Reviews* **7**, 22–44 (2013).